

Cite this: *J. Mater. Chem. B*, 2021,
9, 349

Zwitterionic liquid crystalline polythiophene as an antibiofouling biomaterial†

Jinjia Xu, *^a Jian Xu, ^a Haesoo Moon,^a Herman O. Sintim ^b and Hyowon Lee *^a

To address a key challenge of conjugated polymers in biomedical applications having poor antifouling properties that eventually leads to the failure and reduced lifetime of bioelectronics in the body, herein we describe the design, synthesis, and evaluation of our newly designed multifunctional zwitterionic liquid crystalline polymer **PCBTh-C8C10**, which is facilely synthesized using oxidative polymerization. A conjugated polythiophene backbone, a multifunctional zwitterionic side chain, and a mesogenic unit are integrated into one segment. By DSC and POM characterization, we verify that the introduction of 3,5-bis(2-octyl-1-dodecyloxy)benzene as a mesogenic unit into the polythiophene backbone allows the formation of the liquid crystalline mesophase of the resulting polymer. We also demonstrate that the **PCBTh-C8C10** coated surface exhibits good conductivity, stability, hydrophilicity, and remarkable antibiofouling properties against protein adsorption, cell growth, and bacteria attachment. This new zwitterionic liquid crystalline polymer having good antibiofouling features will be widely recognized as a promising biomaterial that is applicable in implantable organic bioelectronics *via* inhibiting the foreign body response. A deep understanding of structure–property relationships of zwitterionic conjugated polymers has also been provided in this study.

Received 20th September 2020,
Accepted 13th November 2020

DOI: 10.1039/d0tb02264k

rsc.li/materials-b

1. Introduction

π -Conjugated liquid crystals (LCs) have attracted considerable attention due to their ease of anisotropic interaction among mesogens, which generates distinctive behaviours that are difficult to achieve in crystalline materials.^{1–4} LC materials formed by π -conjugated molecules generally self-organize into an ordered supramolecular architecture, giving rise to the formation of various mesophases through strong π - π interactions between the poly-aromatic cores.^{5–11} As such, π -conjugated liquid crystalline polymer materials are emerging as promising semiconducting soft materials because of their ability to form one-dimensionally ordered nanostructures and have the capability to reduce the grain boundary and structural defects for the formation of homogenous thin films, which are essential for the improvement of carrier-transport properties in the device performance.^{12–15} Designing side chains and/or new mesogenic units has recently emerged as an effective and general method to access liquid crystalline mesophases

of conjugated polymers, allowing greater control over crystalline morphologies and improving related device performance.^{16–21} While promising potentials across a variety of applications are constantly being developed, many of them are struggling to maintain reliable functionality in complex *in vivo* environments over time due to the non-specific adsorption of bio-macromolecules on biomedical device surfaces (*i.e.*, biofouling) that reduce the sensitivity and performance of bioelectronic interfaces.^{22–26} The zwitterionic polymers have been reported to be able to prevent non-specific bonding *via* the formation of a hydration layer to serve as a barrier between biomolecules and their surfaces.^{27–42} Recently, our group reported zwitterionic conductive polymers that were demonstrated to have superior antibiofouling properties, biocompatibility, and porosity.²⁸ Using LC mesophases to optimize morphologies of conjugated polymers is attractive as they allow for the precise control over mesoscale features from the nano- to the macroscale using simple and easy processing techniques.^{42–45} However, there still remain challenges to create conjugated polymers that simultaneously exhibit liquid crystalline mesophases as well as good antibiofouling features due to limitations in molecular design and synthetic difficulties.

In this work, we report the design, synthesis, and characterization of a newly designed zwitterionic liquid crystalline polymer **PCBTh-C8C10**, consisting of a conjugated polythiophene backbone, a multifunctional zwitterionic side chain, and a mesogenic unit that are integrated into one segment. Using DSC

^a Weldon School of Biomedical Engineering, Birk Nanotechnology Center, Center for Implantable Devices, Purdue University, West Lafayette, IN 47906, USA. E-mail: xu1267@purdue.edu, hwlee@purdue.edu

^b Department of Chemistry, Center for Drug Discovery, Purdue Institute of Inflammation, Immunology and Infectious Disease, Purdue University, West Lafayette, IN 47906, USA

† Electronic supplementary information (ESI) available. See DOI: 10.1039/d0tb02264k

and POM measurements, we verified that the introduction of 3,5-bis(2-octyl-1-dodecyloxy)benzene as a mesogenic unit into a polythiophene backbone allows the formation of a liquid crystalline mesophase of the resulting polymer. Furthermore, the zwitterionic side chain functionality makes **PCBTh-C8C10** exhibit remarkable antibiofouling properties against protein adsorption, cell adhesion, and bacteria attachment while maintaining good conductivity. This newly developed zwitterionic liquid crystalline polymer **PCBTh-C8C10** can be used as a multifunctional protective layer coated onto the surface of bioelectronic devices, thereby potentially prolonging the lifetime of implantable biomedical devices. The impact of such a structural change on mesostructures as well as antibiofouling properties is studied herein.

2. Experimental section

2.1. Raw materials

1,1'-Carbonyldiimidazole (CDI), 4-bromothiophene-3-carboxylic acid, *N*-hydroxysuccinimide (NHS) and tris(2-carboxyethyl) phosphine hydrochloride (TCEP) were purchased from Chem-Impex International (Wood Dale, IL, USA). The thermo-initiator 2,2'-azobis[2-(2-imidazolin-2-yl)propane]dihydrochloride (VA-044) was purchased from Wako Chemicals USA, Inc. (Richmond, VA, USA). Anhydrous tetrahydrofuran (THF), anhydrous chloroform, methanol, anhydrous dichloromethane, anhydrous toluene, anhydrous *N,N*-dimethylformamide, ethyl acetate, acetonitrile, cystaminedihydrochloride, *N,N'*-dimethylethylenediamine, ethyl bromoacetate, *N*-bromosuccinimide (NBS), boron tribromide, triphenylphosphine, 2-octyl-1-dodecanol, anhydrous FeCl₃, tetrakis(triphenylphosphine)palladium(0), sodium carbonate, potassium carbonate, sodium hydroxide, and glucose were purchased from Sigma-Aldrich (St. Louis, MO, USA). All chemicals were used as received without further purification. Milli-Q water (18.2 MW cm⁻¹, Burlington, MA) was used. Air and water sensitive synthetic manipulations were carried out under an N₂ atmosphere using standard Schlenk techniques. Human cerebral cortex astrocytes, astrocyte medium, cell freezing medium, fetal bovine serum, astrocyte growth supplement, and penicillin/streptomycin solution were purchased from ScienCell Research Laboratories (Carlsbad, CA). CellTracker™ green CMFDA dye, phosphate-buffered saline (PBS, 10×, pH 7.4), albumin from bovine serum fluorescein conjugate (FITC-BSA), Dulbecco's phosphate-buffered saline (no calcium, no magnesium) (DPBS), poly-D-lysine, and the LIVE/DEAD BacLight Bacterial Viability Kit were purchased from ThermoFisher Scientific (Waltham, MA). Tryptic soy broth (TSB) was purchased from Becton Dickinson (Franklin Lakes, NJ). Diced microscope slides and cover glass from Fisher Scientific (Pittsburgh, PA) were used as glass substrates after cleaning with acetone and drying.

2.2. Instruments

¹H-NMR spectra were recorded on a JEOL ECS-500 (500 MHz) spectrometer by using tetramethylsilane (0 ppm for ¹H NMR) as an internal standard. UV-vis absorption spectra were recorded

on a JASCO V-670 spectrophotometer in a quartz cuvette of 1 mm path length. The PerkinElmer LS 55 fluorescence spectrometer was used to collect the fluorescence emission spectra of polymers in solution and film states. The surface morphology was captured using Hitachi S-4800 Field Emission scanning electron microscope (SEM) with 5 kV as the accelerating voltage, and analysed using ImageJ. Electrochemical analysis of polymers was performed using an SP-200 potentiostat (Biologic USA, LLC, Knoxville, TN, USA). The polymer thin-films were coated on the surface of the working electrode. All electrochemical experiments were performed in a conventional three electrode cell configuration in 1× PBS (pH 7.0) as the supporting electrolyte (50 mL for all experiments). A scan rate of 100 mV s⁻¹ and a sampling interval of 1 mV s⁻¹ were used for cyclic voltammetry (CV). Differential scanning calorimetry (DSC) measurements were performed on a DSC Model TA Q-20 under a flowing nitrogen atmosphere. The sample was encapsulated in a sealed aluminium pan, and an identical empty pan was used as the reference. The DSC data were obtained during the second heating/cooling cycles at a scan rate of 10 °C min⁻¹ in the temperature range of 0 °C to 150 °C. A polarizing optical microscope (POM) Nikon ECLIPSE E200 equipped with a Mettler FP82HT hot stage was used for visual observations.

2.3. Preparation of polymer thin-films

The grafting to method was employed to fabricate the thin-films of the polymer. The polymers were dissolved in methanol at a concentration of 10 mg mL⁻¹, followed by the deposition of 100 μL of polymer methanol solution on a clean glass substrate. Then it was left undisturbed until the solvent evaporated at room temperature. The samples were washed with PBS buffer solution five times and dried with filtered air prior to further characterization.

2.4. Protein adsorption study

The antibiofouling performance of polymer-coated surfaces against protein was tested by comparing the fluorescence intensity of respective samples incubated with BSA-FITC. Pristine samples, and **PCBTh** coated, and **PCBTh-C8C10** coated cover glasses were incubated with BSA-FITC in 1× PBS solution of various concentrations in 6-well plates for 4 hours. Then, samples were gently rinsed with 1× PBS solution to remove unabsorbed protein before capturing images by using a fluorescence microscope (Axio Observer Z1, Carl Zeiss Microscopy, Jena, Germany) with a filter set 17 (excitation, BP 485/20, and emission BP 515-565, Carl Zeiss Microscopy, LLC). We used ImageJ to quantify the Image fluorescence intensities.

2.5. Cell attachment

Here we chose astrocyte medium containing 500 mL of basal medium, 10 mL of fetal bovine serum (FBS, Cat. No. 0010), 5 mL of astrocyte growth supplement (AGS, Cat. No. 1852), and 5 mL of penicillin/streptomycin solution (P/S, Cat. No. 0503). Human cerebral cortex astrocytes were cryopreserved at passage one. Astrocytes were expanded and maintained as per ScienCell's

protocol. Astrocytes were cultured in 12-well, tissue culture-treated plates, with 1×10^5 cells seeded per well. These cultures were then incubated until confluent (48 h) in a humidified atmosphere with 5% CO_2 at 37 °C. The medium was replaced one day after seeding. Cells were stained with CellTracker™ Green CMFDA. We replaced the cell culture medium in each well with a 1:1000 ratio of dye to medium with incubation at 37 °C for 30 min.

2.6. Bacterial attachment and biofilm formation array

The antibiofouling performance of polymer-coated surfaces against bacteria was examined by comparing the coverage of live and dead bacteria on the respective samples incubated with *Staphylococcus aureus* (*S. aureus*). We used erythromycin-resistant *S. aureus* tagged with green fluorescent protein (GFP). Prior to each experiment, bacteria cultures were refreshed from stocks in 19:1:0.02 (v/v/v) TSB: 20% (w/v) glucose:erythromycin medium at 37 °C for 12 h at 250 rpm. Then bacteria cultures were diluted to 1/1000 in the same growth medium. In order to start the biofilm growth, 5 mL of the bacteria solution was then aliquoted to each sample, which was previously incubated in 5 mL of 1:9 (v:v) poly-D-lysine: 1× PBS solution for 12 h at room temperature to improve bacteria attachment. After incubation at 37 °C for 48 h at 50 rpm, 1.5 μL propidium iodide (PI) from the Bacterial Viability Kit was added to stain the dead bacteria. After the aspiration of bacteria solution and suitably air drying, the biofilms were imaged using a confocal laser scanning microscope (ZEISS LSM 880, Carl Zeiss, Jena, Germany). Z-Stack images at 100× magnification were taken and analysed using Zeiss Zen software and MATLAB.

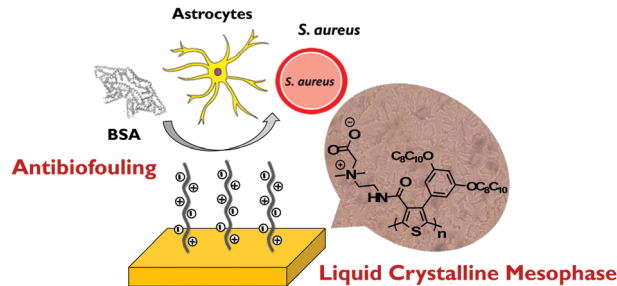
2.7. Statistical analysis

All values are reported as average \pm standard deviation. Statistical analysis was performed using one-way analysis of variance (ANOVA) with Bonferroni correction using OriginPro 2018 software (Northampton, MA). A *p*-value lower than 0.05, 0.01, and 0.005 was denoted as *, **, and ***, respectively.

3. Results and discussions

3.1. Polymer design, synthesis, and characterizations

As has been reported, the zwitterionic side chain attachment has been extensively studied and used as a soft segment in the development of novel biomaterials, which can effectively induce antibiofouling properties and increase the biocompatibility.²⁸ In our study, we designed and synthesized a multifunctional zwitterionic liquid crystalline polymer **PCBTh-C8C10**, which combines a conjugated polythiophene backbone, zwitterionic side chain and a mesogenic unit 3,5-bis(2-octyl-1-dodecyloxy)benzene. As depicted in Scheme 1, we chose conjugated polythiophene as the conjugated backbone due to its good electrical conductivity, chemical stability, and unique electronic and optical properties.⁴⁶ Zwitterionic carboxybetaine was selected as the side chain because of its excellent antibiofouling properties, good water solubility, and biocompatibility. The π -conjugated units



Scheme 1 The illustration of design and molecular structure of polymer **PCBTh-C8C10** in this study, which has superior antibiofouling properties against protein adsorption, cell growth, and bacteria attachment.

attached with long alkoxy side chains have attracted much interest because of their ability to self-assemble and form a mesophase.^{1,2,5-8} It has been reported that the stacking behaviour of π -conjugated units provides opportunities for materials with one-dimensional transport processes, such as energy migration, electric conductivity, and photoconductivity. Because of 3,5-bis(2-octyl-1-dodecyloxy)benzene substituted at the 2-position on thiophene, monomer 5 would possess good solubility, miscibility, and the ability to self-organize into liquid crystalline mesophases that allows for precise control over desirable mesoscale features of the resulting polymers. The synthetic routes for monomer 5 and polymer **PCBTh-C8C10** are summarized in Fig. 1A. Compound 2 was synthesized from commercially available materials 4-bromothiophene-3-carboxylic acid according to a modified literature procedure (Fig. 1A).²⁸ Then compound 4 was synthesized by Williamson reaction of precursor 3, which was prepared by demethylation reaction of 3,5-dimethoxyphenylboronic acid pinacol ester. Subsequent treatment of compound 4 with compound 2 under Suzuki coupling reaction conditions produced the zwitterionic side chain functionalized thiophene monomer 5. The **PCBTh-C8C10** polymer was then prepared from monomer 5 under oxidative polymerization in anhydrous chloroform using ferric chloride as the oxidant.⁴⁷ The resulting polymer **PCBTh-C8C10** was a yellow powder with good solubility in common organic solvents such as chloroform, methanol, and dichloromethane. The chemical structures of pure products were fully characterized and identified by using ¹H and ¹³C nuclear magnetic resonance (NMR) spectroscopy (ESI[†]). The molecular structure of the reference polymer **PCBTh** was also included in Fig. 1B.

3.2. Photophysical and electrochemical properties of polymers

First, we systematically investigated the photophysical and electrochemical properties of **PCBTh-C8C10**. The UV-vis absorption spectra of polymers in solution and in thin solid film states are shown in Fig. 2. Significantly, one intense absorption peak of **PCBTh-C8C10** was observed in the visible range with an absorption maximum at 367 nm (solid line) in methanol solution at 298 K. This characteristic absorption band can be reasonably assigned to the π - π^* transition of the polythiophene backbone.¹² While one additional absorption

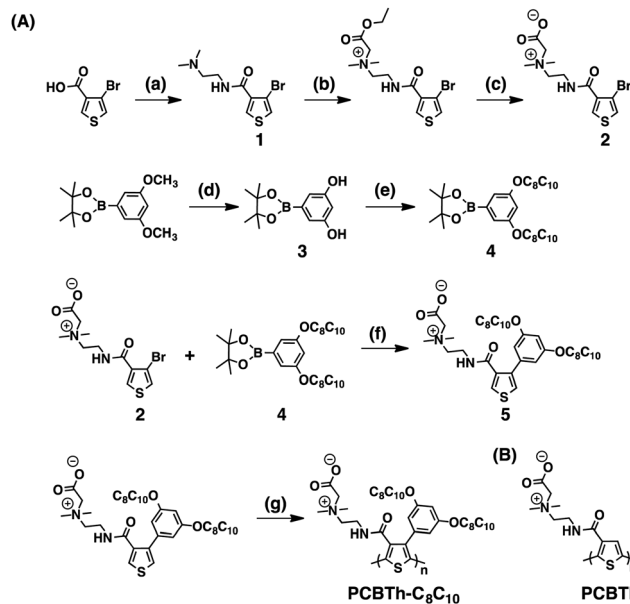


Fig. 1 (A) Synthetic routes for monomer **5** and polymer **PCBTh-C8C10**. Reagents and conditions: (a) 1,1'-carbonyldiimidazole (CDI), *N,N'*-dimethylethylenediamine, THF, 0 °C, 24 h; (b) ethyl bromoacetate, 60 °C, 2 days; (c) NaOH, H₂O; (d) BBr₃, DCM, 0 °C; (e) C₈C₁₀Br, K₂CO₃, DMF, 90 °C, 48 h; (f) Pd(PPh₃)₄, Na₂CO₃, toluene, H₂O, EtOH, reflux, overnight; (g) FeCl₃, CHCl₃, 24 h. (B) The molecular structure of the reference polymer **PCBTh**.

peak of **PCBTh-C8C10** appeared in its thin-film state (dashed line), which undergoes a 49 nm blue-shift relative to the results from methanol solution spectra with a maximum absorption band at 318 nm. Optical bandgaps (E_g) between the energy levels of the highest occupied molecular orbital (E_{HOMO}) and the lowest unoccupied molecular orbital (E_{LUMO}) of **PCBTh-C8C10** estimated from the absorption edge in the film state were 2.49 eV (Fig. 2) compared with the results of 3.59 eV from **PCBTh**.²⁸ The difference in the absorption spectra and optical bandgaps between **PCBTh** and **PCBTh-C8C10** is probably responsible from the electron donating feature of 3,5-bis(2-octyl-1-dodecyloxy)benzene group. Similar to **PCBTh**, the fluorescence emission from **PCBTh-C8C10** was negligible in solution and

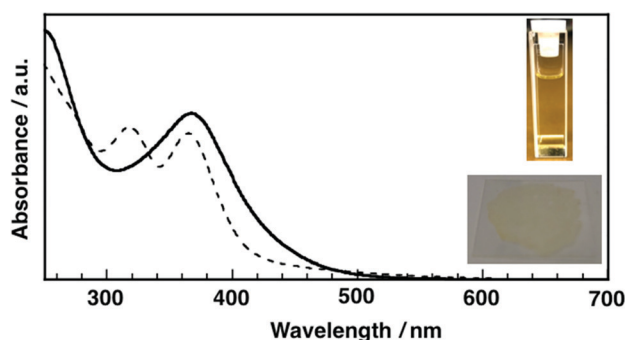


Fig. 2 Normalized UV-vis absorption spectra of **PCBTh-C8C10** dissolved in methanol solution (solid lines) and in thin-film states as deposited (dashed lines) at room temperature. Inset: Photos of polymers dissolved in methanol solution and cast thin-films.

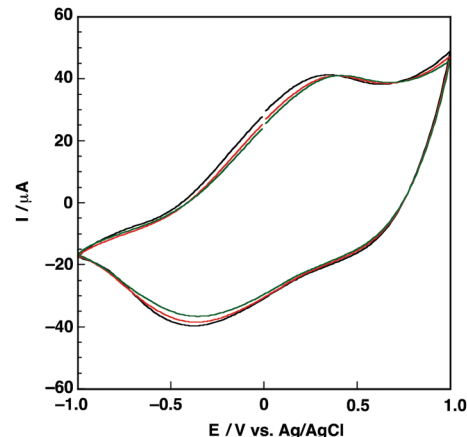


Fig. 3 Cyclic voltammograms of **PCBTh-C8C10** thin-films with scan rate of 100 mV S⁻¹ (first three cycles).

film states (Fig. S1, ESI[†]). In order to be used as novel biomaterials, it is of great essence to have such low fluorescent background when it is regarded as biological matrices especially during the evaluation of its corresponding antibiofouling properties. Cyclic voltammetry (CV) measurements were used to investigate the electrochemical properties of thin-film **PCBTh-C8C10** and **PCBTh** polymers (Fig. 3 and Fig. S2, ESI[†]), which showed comparable overall electrical conductivity relative to previously reported zwitterionic polymers.

3.3. Liquid crystalline behaviour

The thermal phase behavior of **PCBTh-C8C10** was examined *via* differential scanning calorimetry (DSC), whereas the thermotropic liquid crystalline behavior was investigated by using temperature-controlled polarizing optical microscopy (POM). Compared with the DSC results from **PCBTh** that has the

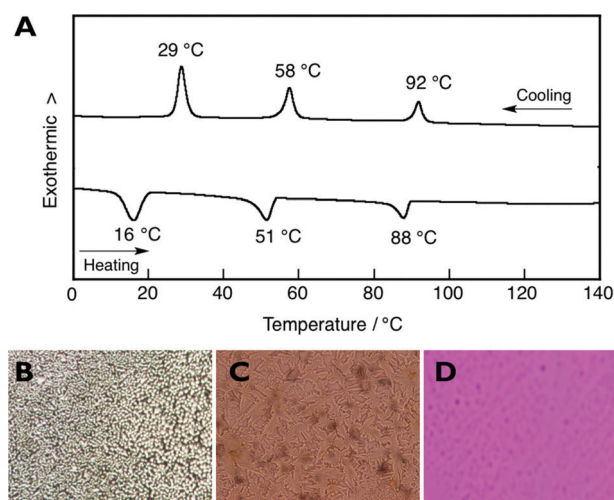


Fig. 4 (A) Differential scanning calorimetry (DSC) trace of **PCBTh-C8C10** in the second sweep with a heating and cooling scan rate of 10 °C min⁻¹; polarized optical microscope (POM) images of **PCBTh-C8C10** of thin films cast from its methanol solution under different temperatures: (B) at 29 °C, (C) at 59 °C and (D) at 95 °C.

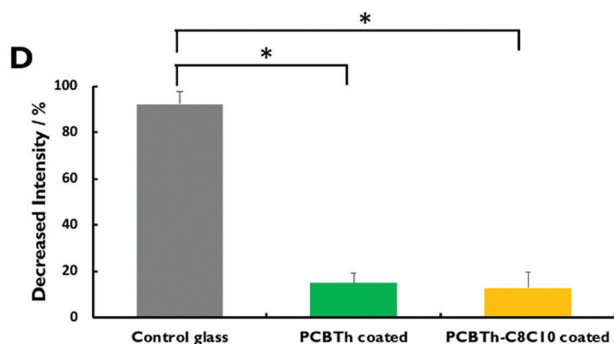
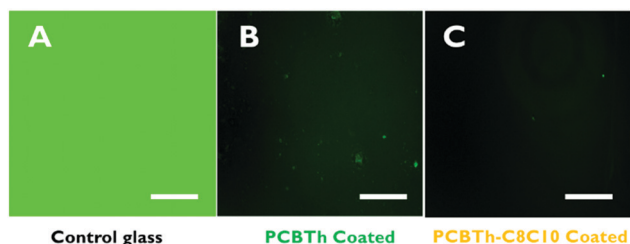


Fig. 5 Fluorescence images of BSA-FITC (A) on pristine glass surface; (B) on PCBTh coated glass surface; and (C) on PCBTh-C8C10 coated glass surface; (scale bar: 200 μm). (D) Comparison of decreased fluorescence intensity. $n = 3$ for each sample, calculated using one-way ANOVA with the Bonferroni test.

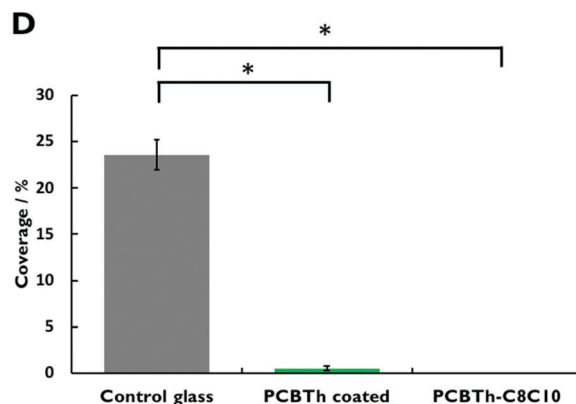
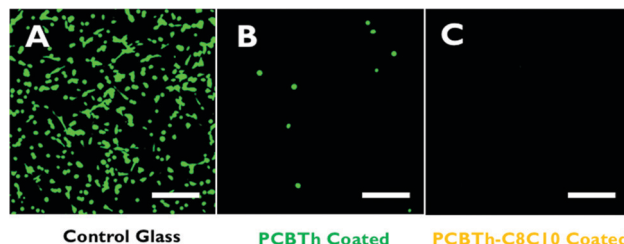


Fig. 6 Representative fluorescence microscopy images of astrocytes cells attached on (A) pristine glass substrate; (B) PCBTh-coated glass surface; (C) PCBTh-C8C10 coated glass surface after 48 h incubation in PBS buffer solution (scale bar: 200 μm); (D) percentage of cell coverage on the surfaces with different treatments. $n = 3$ for each sample, calculated using one-way ANOVA with the Bonferroni test.

amorphous property,²⁸ PCBTh-C8C10 bearing a mesogenic unit at peripheral positions exhibited remarkable π -stacking to form ordered LC assemblies. As shown in Fig. 4A, the DSC measurements of PCBTh-C8C10 from 0 $^{\circ}\text{C}$ to 140 $^{\circ}\text{C}$ revealed the presence of phase transition from an isotropic liquid to a LC phase at 58 $^{\circ}\text{C}$. The following phase transition was found at 29 $^{\circ}\text{C}$, suggesting the crystallization behaviour of PCBTh-C8C10 (Fig. 4B). The POM images of PCBTh-C8C10 exhibited fan-shaped textures at LC mesophases upon cooling from the isotropic liquid at around 58 $^{\circ}\text{C}$, which is the typical observation assigned for smectic LC assemblies (Fig. 4C). Further heating to over 98 $^{\circ}\text{C}$ led to the disappearance of the birefringence, which corresponds to the transition into the isotropic liquid phase (Fig. 4D). The observation of the liquid crystalline texture indicated a smectic liquid crystalline structural formation, which is very similar to that of previously reported liquid crystalline polythiophene.¹² On the other hand, PCBTh did not show any distinct mesophases in both DSC and POM analyses, which suggested the importance of increased interaction between main chain and side mesogenic group attachments. The scanning electron microscopic observation also allows us to directly visualize the nanotexture of PCBTh-C8C10 (Fig. S3, ESI†).

3.4. Protein adsorption study

It has been widely known that protein adsorption on the surface of implantable biomedical devices plays an important role in initiating and regulating foreign body response, blood coagulation, and/or inflammation, which will influence the functional performance and service lifetime of materials and devices.⁴⁸ It is envisioned that zwitterionic CB moieties can dramatically inhibit nonspecific protein adsorption and attachment on biomedical devices.

Thus, we are motivated to test the protein adsorption on our PCBTh-C8C10 polymer coated glass substrates. In order to demonstrate the anti-protein properties of PCBTh-C8C10 coated surfaces, a commonly used protein bovine serum albumin (BSA) was utilized for this study. As in our previous finding²⁴ that the fluorescence intensity of adsorbed BSA-FITC gradually increased and became saturated at a concentration of 6 mg mL^{-1} in PBS, to investigate the antibiofouling capability against the BSA-FITC attachment, we incubated various testing samples in the presence and absence of polymer coatings in BSA-FITC solution (6 mg mL^{-1}) for 4 h, and then

Table 1 The fluorescence intensity of the protein adhesion and the coverage of cell attachment on pristine and polymer-coated glass surfaces are measured and summarized ($n = 3$)

	Control glass	PCBTh coated	PCBTh-C8C10 coated
Decreased fluorescence intensity of BSA	92.3 ± 5.6	15.1 ± 4.1	12.8 ± 6.9
% of astrocytes coverage	23.6 ± 1.6	0.54 ± 0.2	0.006 ± 0.001

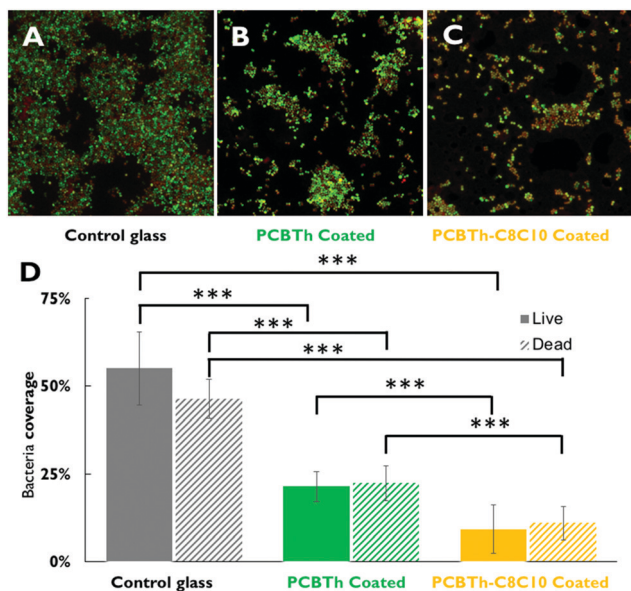


Fig. 7 Representative confocal laser scanning microscopy (CLSM) images of *S. aureus* incubated on (A) pristine glass substrate; (B) PCBTh-coated glass surface; (C) PCBTh-C8C10 coated glass surface for 48 h (scale bar: 20 μ m); (D) quantitative percentages of bacteria coverage on these surfaces. $n = 3$ for each sample, calculated using one-way ANOVA with the Bonferroni test.

evaluated the amount of adsorbed protein on pristine *versus* polymer-coated glass substrates. Under fluorescence microscopic observations, we captured images of each sample and quantified the fluorescence intensity using ImageJ. As shown in Fig. 5A–C, the fluorescence intensity of PCBTh-C8C10 coated surface was significantly reduced up to 87.2% compared to the pristine glass substrate. This decrease in protein adsorption was calculated to be slightly higher BSA-FITC reduction than that observed from PCBTh of 84.9%. The differences in fluorescence intensity between the pristine glass substrates, PCBTh and PCBTh-C8C10 coated surfaces are summarized in Fig. 5D and Table 1. It is also worth noting that these results have good reproducibility and consistency. Similar to other reports claiming that strong hydration of zwitterionic materials provides effective protective layers to prevent biomacromolecules from interacting with the material surface, these results demonstrated that PCBTh-C8C10 coated surface highly resist protein adsorption.

3.5. Cell growth study

For promising implantable biomedical devices, protein adsorption on their surfaces from blood can cause platelet, fibroblast, and astrocyte attachment.⁴⁹ Such kind of attachment easily

leads to foreign body response, resulting in inflammation around implantable materials and biomedical devices. To further demonstrate the antibiofouling properties of polymer PCBTh-C8C10, cell adhesion experiments have been performed by using astrocytes, which are important immunological components of the central nervous system, participating in synaptic plasticity and information processing in the neuronal circuit. The interaction between astrocytes and neurons plays a crucial role in the development and progression of diverse neurological disorders. The astrocyte cultures were incubated to reach confluency for 48 h in a humidified atmosphere with 5% CO₂ at 37 °C. The cell culture medium was replaced one day after seeding. After incubation for 48 h, the control surface of the uncoated glass substrate demonstrated a full coverage of 23.58% of astrocyte cells (Fig. 6A) while minimal cells were found on the PCBTh coated glass substrate and complete inhabitation of cells adhesion was visualized on the PCBTh-C8C10 coated glass substrate (Fig. 6B and C). The coverage of astrocyte cells on the PCBTh and PCBTh-C8C10 coated surfaces was evaluated to be 0.54% and 0.006%, respectively (Fig. 6D and Table 1). These results support our hypothesis that zwitterionic polymer coated surfaces can effectively resist adherent cell attachments as well. More *in vivo* studies of biocompatibility of PCBTh-C8C10 is underway in our lab.

3.6. Biofilm formation *in vitro* arrays

Another major issue of implantable biomedical devices is the risk of infection that will likely cause implant failure. The ability of *Staphylococcus aureus* (*S. aureus*) bacteria to adhere and proliferate on implantable biomedical devices is regarded as one of the major challenges in biomedical fields. As is well known, the infections may be avoided by inhibiting the initial adhesion of bacteria to the substrate surface, thus eliminating the possibility for an infection to occur on the surface of implants and diffuse to the surrounding areas. The new biomaterials with outstanding antibiofouling properties against bacterial attachment and biofilm formation are highly desirable. Thus, we also explored the antimicrobial properties of our polymer PCBTh-C8C10 by using *S. aureus* as a model strain. The adherent bacteria coverage was quantified after incubation of glass samples with and without PCBTh-C8C10 polymer coatings in the *S. aureus* culture solution at 37 °C for 48 h. In order to evaluate whether these polymers coated surface had the potential to inhibit *S. aureus* adhesion and growth, confocal laser scanning microscopy was used to quantify the coverage of live (green) and dead (red) bacteria on various glass samples following the incubation period. As shown in Fig. 7B and C, our results suggest that the glass substrate coated with PCBTh can effectively inhibit *S. aureus*

Table 2 The percentages of *S. aureus* coverage on pristine and polymer-coated surfaces are measured and summarized ($n = 3$)

Control glass		PCBTh coated		PCBTh-C8C10 coated	
Live <i>S. aureus</i> (%)	Dead <i>S. aureus</i> (%)	Live <i>S. aureus</i> (%)	Dead <i>S. aureus</i> (%)	Live <i>S. aureus</i> (%)	Dead <i>S. aureus</i> (%)
55.15 ± 10.46	46.41 ± 5.69	21.40 ± 4.23	22.34 ± 4.95	9.13 ± 2.95	10.91 ± 3.66

attachment during the 48 h incubation. Similarly, the **PCBTh-C8C10** coated surface exhibited a significant reduction in bacterial growth compared to the non-coated control glass substrate (Fig. 7A–C). The amount of *S. aureus* on each surface is summarized in Fig. 7D and Table 2. Our results showed that the zwitterionic liquid crystalline polymer **PCBTh-C8C10** coated surface possess a great capability to resist bacterial adhesion and colonization of biofilm-forming bacteria.

4. Conclusions

In conclusion, a new zwitterionic polymer **PCBTh-C8C10**, consisting of a conjugated polythiophene backbone, a zwitterionic side chain and a mesogenic unit was designed and synthesized by oxidative polymerization. We found that the introduction of 3,5-bis(2-octyl-1-dodecyloxy)benzene mesogenic unit into the polythiophene backbone can facilitate the formation of thermotropic LC assemblies of the resulting polymer. The characterization by DSC and POM revealed that a thermotropic highly ordered mesophase was formed. Liquid crystalline mesophases arising from branched side chains in **PCBTh-C8C10** exhibited favourable control over macroscale structures, crystalline fraction, and molecular patterning, ultimately allowing for further utilization as novel biomaterials. In addition, we demonstrated that the **PCBTh-C8C10** polymer coated surface exhibited remarkable antibiofouling features against protein adsorption, cell adhesion as well as bacterial attachment. The study we present here will pave new avenues in the development of semiconducting soft biomaterials and contribute to the rapidly growing field of implantable bioelectronics.

Conflicts of interest

There are no conflicts to declare.

Acknowledgements

This work was supported in part by the National Science Foundation (United States) under Grants ECCS-1944480 and CNS-1726865, the Global Research Outreach program of Samsung Advanced Institute of Technology, and the Eli Lilly Connected Care Program. The authors are grateful to Dr Bryan Boudouris for allowing access to his laboratory during the polymer synthesis. The authors would also like to thank Dr Lynne Taylor for the access to the polarizing optical microscope (POM). The authors would also like to thank Mr Jim Nolan for his assistance with cell culture experiments.

Notes and references

- 1 S. Kumar, *Taylor and Francis in Chemistry of Discotic Liquid Crystals: From Monomers to Polymers*, CRC Press, Boca Raton, FL, 2011.
- 2 J. W. Goodby, P. J. Collings, T. Kato, C. Tschierske, H. Gleeson and P. Raynes, *Handbook of Liquid Crystals*, Wiley-VCH, Weinheim, Germany, 2nd edn, 2014.
- 3 I. McCulloch, M. Heeney, C. Bailey, K. Genevicius, I. Macdonald, M. Shkunov, D. Sparrowe, S. Tierney, R. Wagner, W. Zhang, M. L. Chabinye, R. J. Kline, M. D. McGehee and M. F. Toney, *Nat. Mater.*, 2006, **5**, 328–333.
- 4 H. Iino and J. Hanna, *Adv. Mater.*, 2011, **23**, 1748–1751.
- 5 S. Kumar, *Chem. Soc. Rev.*, 2006, **35**, 83–109.
- 6 S. Laschat, A. Baro, N. Steinke, F. Giesselmann, C. Hagele, G. Scalia, R. Judele, E. Kapatsina, S. Sauer, A. Schreivogel and M. Tosoni, *Angew. Chem., Int. Ed.*, 2007, **46**, 4832–4887.
- 7 S. Sergeev, W. Pisula and Y. H. Geerts, *Chem. Soc. Rev.*, 2007, **36**, 1902–1929.
- 8 T. Wöhrle, I. Würzbach, J. Kirres, A. Kostidou, N. Kapernaum, J. Littscheidt, J. C. Haenle, P. Staffeld, A. Baro, F. Giesselmann and S. Laschat, *Chem. Rev.*, 2016, **116**, 1139–1241.
- 9 Y. Sagara and T. Kato, *Angew. Chem., Int. Ed.*, 2008, **47**, 5175–5178.
- 10 H. Iino, T. Usui and J. Hanna, *Nat. Commun.*, 2015, **6**, 6828–6836.
- 11 S. Saito, S. Nobusue, E. Tsuzaka, C. Yuan, C. Mori, M. Hara, T. Seki, C. Camacho, S. Irle and S. Yamaguchi, *Nat. Commun.*, 2016, **7**, 12094–12101.
- 12 M. Watanabe, K. Tsuchiya, T. Shinnai and M. Kijima, *Macromolecules*, 2012, **45**, 1825–1832.
- 13 C. R. Bridges, M. J. Ford, B. C. Popere, G. C. Bazan and R. A. Segalman, *Macromolecules*, 2016, **49**, 7220–7229.
- 14 C. R. Bridges, M. J. Ford, G. C. Bazan and R. A. Segalman, *ACS Macro Lett.*, 2017, **6**, 619–624.
- 15 C. R. Bridges, M. J. Ford, E. M. Thomas, C. Gomez, G. C. Bazan and R. A. Segalman, *Macromolecules*, 2018, **51**, 8597–8604.
- 16 J. Xu, *Polym. Chem.*, 2019, **10**, 6334–6341.
- 17 J. Xu, *New J. Chem.*, 2020, **44**, 3566–3569.
- 18 G. Lanzani, *Nat. Mater.*, 2014, **13**, 775–776.
- 19 D. Fichou, *Handbook of Oligo- and Polythiophenes*, Wiley-VCH, Weinheim, New York, 1999.
- 20 K. Tsuyoshi, O. Kazuchika, F. Tetsuya and Y. Iwao, *J. Mater. Chem.*, 1994, **4**, 533–536.
- 21 D. Miyajima, F. Araoka, H. Takezoe, J. Kim, K. Kato, M. Takata and T. Aida, *Science*, 2012, **336**, 209–213.
- 22 M. R. Abidian and D. C. Martin, *Adv. Funct. Mater.*, 2009, **19**, 573–585.
- 23 R. A. Green, N. H. Lovell, G. G. Wallace and L. A. P. Warren, *Biomaterials*, 2008, **29**, 3393–3399.
- 24 J. Xu, H. Moon, J. Xu, J. Lim, T. Fischer, H. A. McNally, H. O. Sintim and H. Lee, *ACS Appl. Mater. Interfaces*, 2020, **12**, 26893–26904.
- 25 J. Xu and H. Lee, *Chemosensors*, 2020, **8**, 66–95.
- 26 H. Park, A. H. Raffee, S. W. M. John, A. M. Ardekani and H. Lee, *Microsyst. Nanoeng.*, 2018, **4**, 35–47.
- 27 L. Zheng, H. S. Sundaram, Z. Wei, C. Li and Z. Yuan, *React. Funct. Polym.*, 2017, **118**, 51–61.

- 28 J. Xu, J. Xu, H. Moon, H. O. Sintim and H. Lee, *ACS Appl. Polym. Mater.*, 2020, **2**, 528–536.
- 29 L. Zhang, Z. Cao, T. Bai, L. Carr, J.-R.-E. Menye, C. Irvin, B. D. Ratner and S. Jiang, *Nat. Biotechnol.*, 2013, **31**, 553–557.
- 30 X. Lin, P. Jain, K. Wu, D. Hong, H.-C. Hung, M. B. O’Kelly, B. Li, P. Zhang, Z. Yuan and S. Jiang, *Langmuir*, 2019, **35**, 1544–1551.
- 31 B. Cao, Q. Tang, L. L. Li, C. J. Lee, H. Wang, Y. Q. Zhang, H. Castaneda and G. Cheng, *Chem. Sci.*, 2015, **6**, 782–788.
- 32 B. Cao, C.-J. Lee, Z. Zeng, F. Cheng, F. Xu, H. Cong and G. Cheng, *Chem. Sci.*, 2016, **7**, 1976–1981.
- 33 B. Cao, L. L. Li, H. Y. Wu, T. Qiong, B. B. Sun, H. Dong, J. Zhe and G. Cheng, *Chem. Commun.*, 2014, **50**, 3234–3237.
- 34 H. Wang, Y. Hu, D. Lynch, M. Young, S. Li, H. Cong, F.-J. Xu and G. Cheng, *ACS Appl. Mater. Interfaces*, 2018, **10**, 37609–37617.
- 35 Y. N. Chou, F. Sun, H. C. Hung, P. Jain, A. Sinclair, P. Zhang, T. Bai, Y. Chang, T. C. Wen and Q. Yu, *Acta Biomater.*, 2016, **40**, 31–37.
- 36 Y. Hu, B. Liang, L. Fang, G. Ma, G. Yang, Q. Zhu, S. Chen and X. Ye, *Langmuir*, 2016, **32**, 11763–11770.
- 37 H. Wu, C. J. Lee, H. Wang, Y. Hu, M. Young, Y. Han, F. J. Xu, H. Cong and G. Cheng, *Chem. Sci.*, 2018, **9**, 2540–2546.
- 38 J. Ladd, Z. Zhang, S. Chen, J. C. Hower and S. Jiang, *Biomacromolecules*, 2008, **9**, 1357–1361.
- 39 S. Y. Lee, Y. Lee, P. LeThi, D. H. Oh and K. D. Park, *Biomater. Res.*, 2018, **22**, 3–10.
- 40 L. Mi and S. Jiang, *Angew. Chem., Int. Ed.*, 2014, **53**, 1746–1754.
- 41 S. Chen, J. Zheng, L. Li and S. Jiang, *J. Am. Chem. Soc.*, 2005, **127**, 14473–14478.
- 42 C. M. E. Tan, G. V. Dizon, S.-H. Chen, A. Venault, Y.-N. Chou, L. Tayo and Y. J. Chang, *J. Mater. Chem. B*, 2020, **8**, 8853–8863.
- 43 M. C. Valles, A. M. Bueno, R. Gimenez, T. Sierra and M. B. Ros, *J. Mater. Chem. C*, 2019, **7**, 14454–14470.
- 44 C. R. Snyder, R. J. Kline, D. M. Delongchamp, R. C. Nieuwendaal, L. J. Richter, M. Heeney and I. McCulloch, *J. Polym. Sci., Part B: Polym. Phys.*, 2015, **53**, 1641–1653.
- 45 C. Tschierske, *Chem. Soc. Rev.*, 2007, **36**, 1930–1970.
- 46 S. Das, D. P. Chatterjee, R. Ghosh and A. K. Nandi, *RSC Adv.*, 2015, **5**, 20160–20177.
- 47 X. Pang, P. Imin, I. Zhitomirsky and A. Adronov, *Macromolecules*, 2010, **43**, 10376–10381.
- 48 J. N. Lockhart, T. J. Spoonmore, M. W. McCurdy, B. R. Rogers, S. A. Guelcher and E. Harth, *ACS Appl. Mater. Interfaces*, 2018, **10**, 4050–4056.
- 49 Y.-B. Sun, H. Zhao, D.-L. Mu, W. Zhang, J. Cui, L. Wu, A. Alam, D.-X. Wang and D. Ma, *Cell Death Dis.*, 2019, **10**, 167–180.